

COMMUNICATION



Cite this: *Dalton Trans.*, 2023, **52**, 17679

Received 11th October 2023,
Accepted 10th November 2023

DOI: 10.1039/d3dt03348a

rsc.li/dalton

Carboxyl position-directed structure diversity in zirconium-tricarboxylate frameworks†

Jun Xia,^{a,b} Jincheng Si,^b Kang Zhou,^b Hai-Lun Xia,^b Jian Zhang,^b Yingqian Xu,^{*a} Lei Wang^{*b} and Xiao-Yuan Liu^{ib} ^{*b}

Herein, three tritopic carboxylic acids were used to construct three Zr-MOFs, HIAM-4033, HIAM-4034, and HIAM-4035, to investigate the effect of carboxyl position on the MOF structures. The results showed that HIAM-4033 and HIAM-4034 possess (3,9)-c models with different underlying nets, whereas HIAM-4035 exhibits the same underlying net as UiO-68. Nanosized HIAM-4033 exhibits excellent sensitivity and selectivity for detecting aromatic acids, such as benzoic acid and 2-fluorobenzoic acid, compared with aliphatic acids and inorganic acids. This study offers new insights into achieving an organic linker directed structure evolution of Zr-MOFs, which might facilitate the discovery of unprecedented underlying nets.

Since first reported in 2008,¹ zirconium-based metal-organic frameworks (Zr-MOFs)^{2,3} have been extensively studied and widely used in catalysis, chemical separation and storage, and bio-related areas owing to their great chemical and thermal stability, highly tunable structures, and specific properties.^{4,5} It is clear and interesting that the unlimited choice of carboxylic acid-based organic linkers (ditopic, tritopic, tetratopic, and hexatopic carboxylate linkers with different geometries) endow Zr-MOFs with different underlying topologies and various properties.⁶ It has also been reported that multiple Zr-MOFs with varying topologies can be constructed using the same organic linker, especially for tetratopic carboxylate linkers.^{7–13} For example, tetrakis(4-carboxyphenyl)porphyrin (H₄TCPP) can be used to prepare Zr-MOFs with (4,6)-c she,¹⁴ (4,8)-c csq,¹⁵ (4,8)-c sqc,¹⁶ (4,8)-c scu,¹⁷ (4,12)-c shp,¹⁸ and (4,12)-c ftw¹⁹ underlying topologies. The (4,12)-c ftw,²⁰ (4,8)-c csq,²¹ (4,8)-c scu with 2-fold interpenetration,^{22,23} and (4,12)-c

shp²⁴ type Zr-MOFs can be formed using 4',4''',4''''',4''''''- (ethene-1,1,2,2-tetrayl)tetrakis([1,1'-biphenyl]-4-carboxylic acid) (H₄ETTC) as the organic linker. Although great works have been done to prepare new Zr-MOFs and investigate the linker structure-directed topology evolution of resultant Zr-MOFs,^{25,26} few studies have focused on the position of carboxyl group induced structure diversity.²⁷ Herein, three tritopic carboxylic acids, with carboxyl group located at different positions on the thiophene moiety (Fig. 1), were used to construct Zr-MOFs. As expected, three different structures were obtained using these linkers, which indicated that changing the position of carboxyl group can be a useful strategy to realize the structural evolution of Zr-MOFs and might facilitate the discovery of Zr-MOFs with unique structures.

Three tritopic carboxylic acids, 4,4'-(2-(5-carboxythiophen-2-yl)-1H-benzo[d]imidazole-4,7-diyl)dibenzoic acid (H₃5CIB), 4,4'-(2-(4-carboxythiophen-2-yl)-1H-benzo[d]imidazole-4,7-diyl)dibenzoic acid (H₃4CIB), and 4,4'-(2-(3-carboxythiophen-2-yl)-1H-benzo[d]imidazole-4,7-diyl)dibenzoic acid (H₃3CIB), were designed and synthesized (Fig. 1, detail synthesis routes in the ESI†). Then these three tricarboxylic acid-based Zr-MOFs were prepared using the following method: a 5 mL vial containing

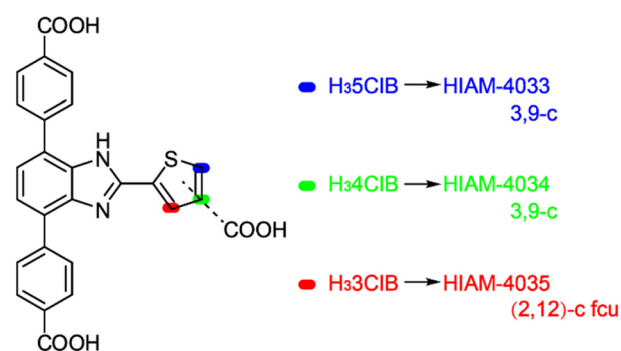


Fig. 1 Molecular structures of tricarboxylate linkers with carboxyl group at different positions of thiophene and the resultant connectivity of Zr₆ cluster in corresponding MOFs.

^aSchool of Chemical Engineering, University of Science and Technology Liaoning, Anshan 114051, P. R. China. E-mail: 319973300071@ustl.edu.cn

^bHoffmann Institute of Advanced Materials, Shenzhen Polytechnic University, 7098 Liuxian Blvd, Nanshan District, Shenzhen 518055, P. R. China. E-mail: wliam@szpu.edu.cn, liuxiaoyuan1989@szpu.edu.cn

†Electronic supplementary information (ESI) available. CCDC 2269047 and 2269048. For ESI and crystallographic data in CIF or other electronic format see DOI: <https://doi.org/10.1039/d3dt03348a>

23.3 mg ZrCl_4 , 10 mg linkers, different volumes of organic acids (formic or trifluoroacetic acid) and organic solvents (DMF or DEF) was placed in a preheated oven at 120 °C for 3 days. Colorless single crystals, HIAM-4033, HIAM-4034, and HIAM-4035, with blue emission under 365 nm excitation were obtained for $\text{H}_3\text{5CIB}$, $\text{H}_3\text{4CIB}$, and $\text{H}_3\text{3CIB}$ -based Zr-MOFs, respectively.

Single-crystal X-ray diffraction (SC-XRD) analysis revealed that HIAM-4033 crystallizes in a trigonal crystal system with $P3_121$ space group (Table S1†). As shown in Fig. 2a and S1–S3,† each Zr_6 cluster is connected by nine fully deprotonated $\text{H}_3\text{5CIB}$ linkers in which six carboxylic groups are from the benzene rings and the other three are located on the thiophene rings (Fig. S2†). Each $\text{H}_3\text{5CIB}$ is coordinated to three Zr_6 clusters (Fig. S3†). As a result, (3,9)-c underlying net is generated in HIAM-4033 with an overall formula of $\text{Zr}_6\text{O}_4(\text{OH})_7(\text{H}_2\text{O})_3(\text{5CIB})_3$.

The SC-XRD measurement indicated that HIAM-4034 also crystallizes in a trigonal crystal system but with an $R32$ space group (Table S2†). As depicted in Fig. 2b and S4–S6,† similar to HIAM-4033, each Zr_6 cluster is coordinated by nine deprotonated $\text{H}_3\text{4CIB}$ linkers in which six carboxylic groups are from the benzene rings and the other three are located on the thiophene rings (Fig. S5†). The difference with HIAM-4033 is that not all of the oxygen atoms on the carboxylic groups are connected to the Zr_6 cluster. Four out of six carboxylic groups located on the benzene rings and two out of three carboxylic groups from the thiophene rings are coordinated with the Zr_6 cluster *via* two oxygen atoms, while all the other carboxylic groups are connected to the Zr_6 cluster *via* a single oxygen atom (Fig. S5†). Each $\text{H}_3\text{4CIB}$ is also coordinated to three Zr_6 clusters (Fig. S6†). As a result, the overall formula of HIAM-4034 is $\text{Zr}_6\text{O}_4(\text{OH})_{10}(\text{H}_2\text{O})_3(\text{4CIB})_3$. Although HIAM-4034

also possesses a (3,9)-c underlying net, it is completely different from that in HIAM-4033. The carboxyl group induced structural evolution contributed to the different linker conformations of $\text{H}_3\text{5CIB}$ in HIAM-4033 and $\text{H}_3\text{4CIB}$ in HIAM-4034, as shown in Fig. S7.†

However, for HIAM-4035, the crystal structure cannot be solved using SC-XRD analysis because of the much smaller crystal size compared with that of HIAM-4033 and HIAM-4034. Fortunately, due to the octagonal-shaped single crystals (Fig. 2c), we envision that (2,12)-c *fcu* topology might be formed using $\text{H}_3\text{3CIB}$ as the organic linker, which is confirmed by the well-matched powder X-ray diffraction (PXRD) patterns between the simulated UiO-68 and the experimental HIAM-4035 (Fig. 3a). These results demonstrate that the position of the carboxylic group has a significant effect on the structures of resultant Zr-MOFs, which offers a useful approach to designing and discovering new MOF structures.

The phase purity of HIAM-4033 to HIAM-4035 was confirmed by the near-identical PXRD patterns of the simulated and experimental samples (Fig. 3a). The solid-state emission and absorption spectra of HIAM-4033 to HIAM-4035 were then measured to investigate the carboxyl position induced differences in optical behavior. As shown in Fig. 3b, the emission maxima are 473, 445, and 483 nm for HIAM-4033, HIAM-4034, and HIAM-4035, respectively, which indicates that the carboxyl position has a significant effect on the emission behaviors of resultant Zr-MOFs. However, the difference in carboxyl positions has a slight effect on the absorption properties of the three MOFs (Fig. 3c). The photoluminescence quantum yields are 22.8%, 10.5%, and 4.7% for HIAM-4033, HIAM-4034, and HIAM-4035, respectively, under 365 nm excitation.

The chemical and thermal stabilities of HIAM-4033 and HIAM-4034 were tested under various conditions to evaluate

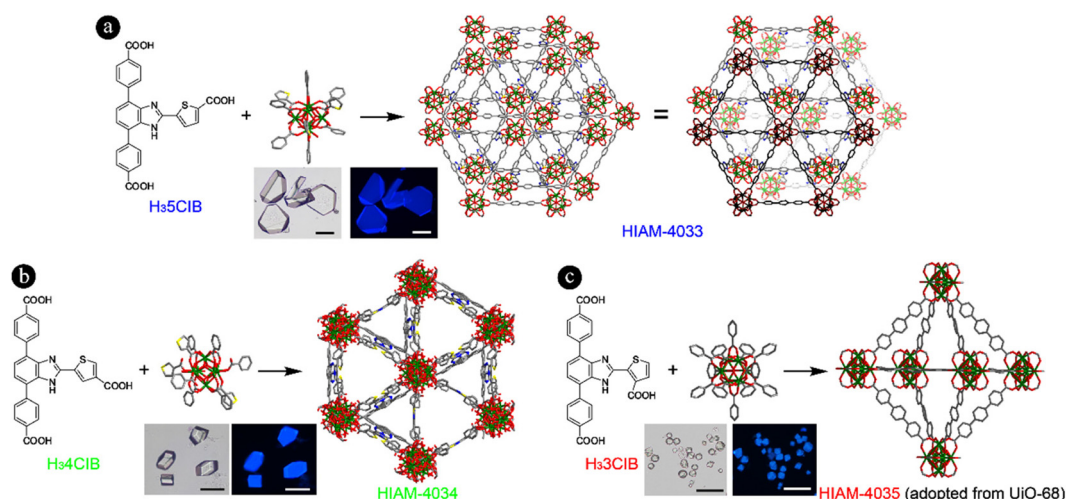


Fig. 2 The molecular structure of $\text{H}_3\text{5CIB}$, Zr_6 cluster, single crystal images of HIAM-4033 under daylight and 365 nm excitation (scale bar: 100 μm) and the single crystal structure of HIAM-4033 (a); the molecular structure of $\text{H}_3\text{4CIB}$, Zr_6 cluster, single crystal images of HIAM-4034 under daylight and 365 nm excitation (scale bar: 50 μm) and the single crystal structure of HIAM-4034 (b); the molecular structure of $\text{H}_3\text{3CIB}$, Zr_6 cluster, single crystal images of HIAM-4035 under daylight and 365 nm excitation (scale bar: 50 μm) and the single crystal structure of HIAM-4035 adopted from UiO-68 (c).

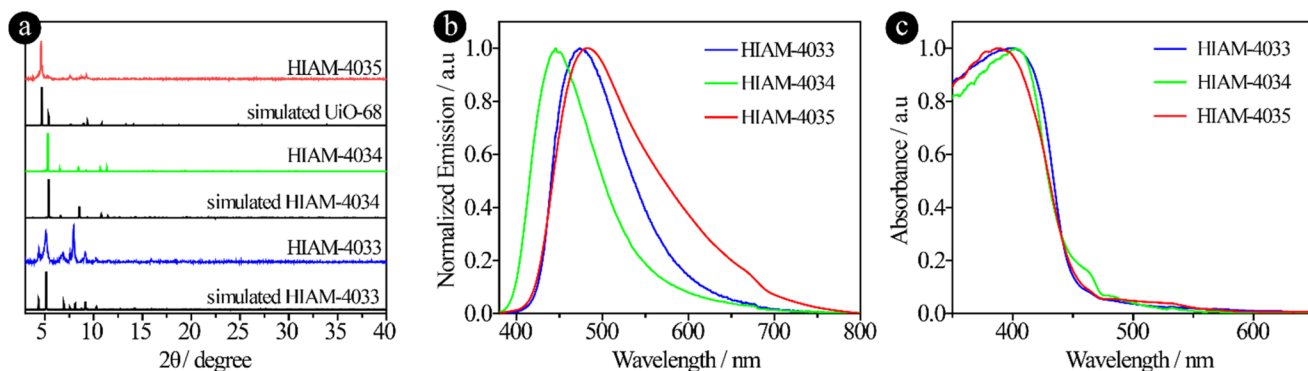


Fig. 3 The PXRD of simulated and experimental HIAM-4033, HIAM-4034 and HIAM-4035 (a); the normalized emission (b) and absorption spectra (c) of HIAM-4033, HIAM-4034 and HIAM-4035.

their suitability for potential real-world applications. The chemical stabilities of HIAM-4033 and HIAM-4034 were explored under different conditions, including soaking in water at room temperature, in boiling water, in 0.001 M NaOH, in 4 M HCl and in concentrated HCl at room temperature for 24 hours. As shown in Fig. S8,[†] the near-identical PXRD patterns of the simulated and experimental HIAM-4033 and HIAM-4034 reveal that both the MOFs maintained their structural integrity very well under all the test conditions. Thermogravimetric analysis (TGA) indicated that HIAM-4033 and HIAM-4034 have high thermal stability at temperatures up to 500 °C (Fig. S9[†]). These results demonstrate that HIAM-4033 and HIAM-4034 have excellent chemical and thermal stability, which is essential for their applications.

Due to the excellent stability and great emission property of HIAM-4033, its potential application as a chemical sensor was explored. The nanosized HIAM-4033 was prepared first because it is important to realize high dispersibility of materials for aqueous phase sensing. As depicted in Fig. S10,[†] HIAM-4033 with size around 500 nm was synthesized. The phase purity of nanosized HIAM-4033 was confirmed by the excellent agreement of simulated and experimental PXRD patterns (Fig. S11[†]).

As reported, MOFs constructed using nitrogen-heterocycle-based emissive linkers exhibit great performance for acid detection.²⁸ Therefore, the aqueous suspension of nanosized HIAM-4033 was utilized for sensing of acids, including aromatic acids [benzoic acid (BA) and 2-fluorobenzoic acid (2-FBA)], aliphatic acids [formic acid (FA), acetic acid (AA), trifluoroacetic acid (TFA) and propionic acid (PA)], and inorganic acids (HCl, HBr, and HNO₃). As shown in Fig. 4a, the remarkable emission enhancement of HIAM-4033 was recorded when BA and 2-FBA were added at concentrations below 200 μM. While, at the same concentration, other acids led to much less fluorescence enhancement. This result demonstrates that nanosized HIAM-4033 can be employed as a highly selective chemical sensor for the detection of aromatic acids in aqueous solution. Then titration experiments were conducted to determine the sensitivity of HIAM-4033 for 2-FBA and BA detection.

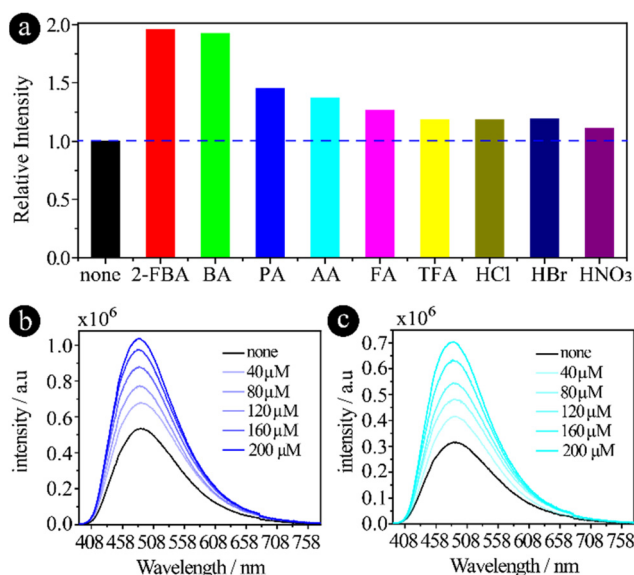


Fig. 4 The selectivity of nanosized HIAM-4033 in aqueous solution toward different types of acids (a); concentration-dependent emission enhancement of nanosized HIAM-4033 for the detection of 2-FBA (b) and BA (c).

The emission intensity of HIAM-4033 gradually increased with increasing 2-FBA and BA concentrations (Fig. 4b and c). Linear correlation coefficients of 0.994 and 0.988 were obtained for 2-FBA and BA detection, respectively, in the concentration range from 40 μM to 200 μM. Accordingly, the detection limits for 2-FBA and BA were calculated to be 1.58 and 2.35 μM, respectively. The above-mentioned results indicate that nanosized HIAM-4033 shows excellent sensitivity and selectivity for aromatic acid detection. The mechanism of aromatic acid detection can be ascribed to the fact that trapped aromatic acids in nanosized HIAM-4033 can restrict the rotation of organic linkers through hydrogen bonding and π - π interaction, which reduces nonradiative recombination and leads to enhanced emission. The hypothesis was further confirmed

by slight emission changes of organic linkers in solution with the gradually increased concentration of aromatic acids (Fig. S12†). The stability of nanosized HIAM-4033 during the detection was confirmed *via* PXRD and SEM. The near-identical PXRD patterns and SEM images before and after the detection of 2-FBA and BA (Fig. S11 and S13†) further reveal the chemical stability of HIAM-4033 and its potential application as a chemical sensor.

In conclusion, carboxyl position induced structure evolution was explored in zirconium-tricarboxylate frameworks. Two (3,9)-c Zr-MOFs, HIAM-4033 and HIAM-4034, with completely different underlying nets and one (2,12)-c UiO-68-type Zr-MOFs, HIAM-4035, were obtained *via* changing the substituted position of carboxyl group in the thiophene moiety of tri-topic carboxylic acids. Nanosized HIAM-4033 shows high performance for the sensitive and selective detection of aromatic acids. This study provides new insights into investigating the organic linker directed structure diversity of Zr-MOFs, which might facilitate the discovery of new Zr-MOFs with unprecedented underlying nets.

Conflicts of interest

There are no conflicts to declare.

Acknowledgements

The authors gratefully acknowledge the support from Shenzhen Polytechnic. X.-Y. Liu acknowledges the financial support from the National Natural Science Foundation of China (No. 22201185), Guangdong Basic and Applied Basic Research Foundation (2023A1515011494), and start-up funding for Shenzhen High-Caliber Personnel of Shenzhen Polytechnic (6022310053K). L. Wang gratefully acknowledges the financial support from Post-doctoral Foundation Project of Shenzhen Polytechnic (6022331004K).

References

- 1 J. H. Cavka, S. Jakobsen, U. Olsbye, N. Guillou, C. Lamberti, S. Bordiga and K. P. Lillerud, *J. Am. Chem. Soc.*, 2008, **130**, 13850–13851.
- 2 Y. Bai, Y. Dou, L. H. Xie, W. Rutledge, J. R. Li and H. C. Zhou, *Chem. Soc. Rev.*, 2016, **45**, 2327–2367.
- 3 Y. Chen, Z. L. Shi, L. Wei, B. Zhou, J. Tan, H. L. Zhou and Y. B. Zhang, *J. Am. Chem. Soc.*, 2019, **141**, 3298–3303.
- 4 S. Yuan, L. Feng, K. Wang, J. Pang, M. Bosch, C. Lollar, Y. Sun, J. Qin, X. Yang, P. Zhang, Q. Wang, L. Zou, Y. Zhang, L. Zhang, Y. Fang, J. Li and H. C. Zhou, *Adv. Mater.*, 2018, **30**, e1704303.
- 5 S. Yuan, J.-S. Qin, C. T. Lollar and H.-C. Zhou, *ACS Cent. Sci.*, 2018, **4**, 440–450.
- 6 H. Ghasempour, K.-Y. Wang, J. A. Powell, F. ZareKarizi, X.-L. Lv, A. Morsali and H.-C. Zhou, *Coord. Chem. Rev.*, 2021, **426**, 213542.
- 7 J. Pang, S. Yuan, J. Qin, C. Liu, C. Lollar, M. Wu, D. Yuan, H. C. Zhou and M. Hong, *J. Am. Chem. Soc.*, 2017, **139**, 16939–16945.
- 8 J. H. Carter, X. Han, F. Y. Moreau, I. da Silva, A. Nevin, H. G. W. Godfrey, C. C. Tang, S. Yang and M. Schroder, *J. Am. Chem. Soc.*, 2018, **140**, 15564–15567.
- 9 X. L. Lv, S. Yuan, L. H. Xie, H. F. Darke, Y. Chen, T. He, C. Dong, B. Wang, Y. Z. Zhang, J. R. Li and H. C. Zhou, *J. Am. Chem. Soc.*, 2019, **141**, 10283–10293.
- 10 Y. Chen, X. Zhang, M. R. Mian, F. A. Son, K. Zhang, R. Cao, Z. Chen, S. J. Lee, K. B. Idrees, T. A. Goetjen, J. Lyu, P. Li, Q. Xia, Z. Li, J. T. Hupp, T. Islamoglu, A. Napolitano, G. W. Peterson and O. K. Farha, *J. Am. Chem. Soc.*, 2020, **142**, 21428–21438.
- 11 H.-L. Xia, K. Zhou, L. Yu, H. Wang, X.-Y. Liu, D. M. Proserpio and J. Li, *Inorg. Chem.*, 2022, **61**, 7980–7988.
- 12 B. Wang, Q. Yang, C. Guo, Y. Sun, L. H. Xie and J. R. Li, *ACS Appl. Mater. Interfaces*, 2017, **9**, 10286–10295.
- 13 X. Li, J. Liu, K. Zhou, S. Ullah, H. Wang, J. Zou, T. Thonhauser and J. Li, *J. Am. Chem. Soc.*, 2022, **144**, 21702–21709.
- 14 D. Feng, W. C. Chung, Z. Wei, Z. Y. Gu, H. L. Jiang, Y. P. Chen, D. J. Darensbourg and H. C. Zhou, *J. Am. Chem. Soc.*, 2013, **135**, 17105–17110.
- 15 D. Feng, Z. Y. Gu, J. R. Li, H. L. Jiang, Z. Wei and H. C. Zhou, *Angew. Chem., Int. Ed.*, 2012, **51**, 10307–10310.
- 16 H. L. Jiang, D. Feng, K. Wang, Z. Y. Gu, Z. Wei, Y. P. Chen and H. C. Zhou, *J. Am. Chem. Soc.*, 2013, **135**, 13934–13938.
- 17 P. Deria, D. A. Gómez-Gualdrón, I. Hod, R. Q. Snurr, J. T. Hupp and O. K. Farha, *J. Am. Chem. Soc.*, 2016, **138**, 14449–14457.
- 18 D. Feng, Z. Y. Gu, Y. P. Chen, J. Park, Z. Wei, Y. Sun, M. Bosch, S. Yuan and H. C. Zhou, *J. Am. Chem. Soc.*, 2014, **136**, 17714–17717.
- 19 W. Morris, B. Voloskiy, S. Demir, F. Gándara, P. L. McGrier, H. Furukawa, D. Cascio, J. F. Stoddart and O. M. Yaghi, *Inorg. Chem.*, 2012, **51**, 6443–6445.
- 20 Z. Wei, Z.-Y. Gu, R. K. Arvapally, Y.-P. Chen, R. N. McDougald Jr., J. F. Ivy, A. A. Yakovenko, D. Feng, M. A. Omary and H.-C. Zhou, *J. Am. Chem. Soc.*, 2014, **136**, 8269–8276.
- 21 Q. Zhang, J. Su, D. Feng, Z. Wei, X. Zou and H.-C. Zhou, *J. Am. Chem. Soc.*, 2015, **137**, 10064–10067.
- 22 C.-X. Chen, Z.-W. Wei, C.-C. Cao, S.-Y. Yin, Q.-F. Qiu, N.-X. Zhu, Y.-Y. Xiong, J.-J. Jiang, M. Pan and C.-Y. Su, *Chem. Mater.*, 2019, **31**, 5550–5557.
- 23 M. J. Hurlock, L. Hao, K. W. Kriegsman, X. Guo, M. O'Keeffe and Q. Zhang, *ACS Appl. Mater. Interfaces*, 2021, **13**, 51945–51953.
- 24 C.-X. Chen, S.-Y. Yin, Z.-W. Wei, Q.-F. Qiu, N.-X. Zhu, Y.-N. Fan, M. Pan and C.-Y. Su, *Angew. Chem., Int. Ed.*, 2019, **58**, 14379–14385.

- 25 V. Guillermin, T. Grancha, I. Imaz, J. Juanhuix and D. MasPOCH, *J. Am. Chem. Soc.*, 2018, **140**, 10153–10157.
- 26 J. Si, H.-L. Xia, K. Zhou, J. Li, K. Xing, J. Miao, J. Zhang, H. Wang, L.-L. Qu, X.-Y. Liu and J. Li, *J. Am. Chem. Soc.*, 2022, **144**, 22170–22177.
- 27 H. Liu, F. Chen, D. Bai, J. Jiao, W. Zhou, T. Yildirim and Y. He, *Cryst. Growth Des.*, 2017, **17**, 248–254.
- 28 J. Qiao, X. Liu, L. Zhang, J. F. Eubank, X. Liu and Y. Liu, *J. Am. Chem. Soc.*, 2022, **144**, 17054–17063.